FISEVIER

Contents lists available at ScienceDirect

# Deep-Sea Research Part I

journal homepage: www.elsevier.com/locate/dsri



# Spatial patterns of benthic silica flux in the North Pacific reflect upper ocean production



Yi Hou<sup>a,\*,1</sup>, Douglas E. Hammond<sup>a</sup>, William M. Berelson<sup>a</sup>, Nathaniel Kemnitz<sup>a</sup>, Jess F. Adkins<sup>b</sup>, Abby Lunstrum<sup>a</sup>

- <sup>a</sup> Department of Earth Sciences, University of Southern California, 3651 Trousdale Pkwy Los Angeles, CA, 90089, USA
- b Division of Geological and Planetary Sciences, California Institute of Technology, MC 170-25, 1200 E. California Blvd. Pasadena, CA, 91125, USA

#### ABSTRACT

Diatoms are the dominant algal group that cycles dissolved silicic acid in the ocean; they also play an important role in the oceanic carbon cycle. It is therefore important to quantify the spatial distribution of silica cycling for defining global ocean biogeochemical cycles. On the research cruise CDisK-IV, water samples and sediment cores were collected at 5 stations along a North Pacific transect near  $150^{\circ}$ W from  $22^{\circ}$ N to  $50^{\circ}$ N to evaluate benthic remineralization rates of biogenic silica (bSi). Two independent methods, core incubation and diffusive transport based on porewater profiles, were utilized to estimate benthic silicic acid fluxes, and these independent methods yield fluxes that agree within uncertainties. The benthic fluxes are reported as  $0.04 \pm 0.01$ ,  $0.04 \pm 0.01$ ,  $0.05 \pm 0.01$ ,  $0.67 \pm 0.14$ ,  $0.40 \pm 0.08$  mmol Si m<sup>-2</sup> day<sup>-1</sup> for Stations 1 to 5, south to north, respectively. Burial fluxes were estimated using measurements of solid phase bSi in sediments and literature values of sediment accumulation rate. Burial efficiencies of bSi at all stations were < 5% and show reasonable agreement with previous estimates. When burial rates were added to benthic fluxes to calculate rain rates, the rain observed under the subarctic gyre (Stations 4–5), was far larger than in the lower latitudes of the subtropics (Stations 1–3), corresponding to higher surface diatom productivity at higher latitudes. At the two northern stations, the bottom 500 m of the water column shows a near-bottom increase in silicic acid that is consistent with the measured benthic flux and the estimated vertical eddy diffusivity. Above this horizon, water column density stratification increases and vertical diffusivity decreases, but the silicic acid gradient decreases. This reduction in gradient indicates that above this horizon, horizontal transport by deep waters, rather than vertical diffusion, becomes the dominant process removing the silicic acid released by benthic remineralization.

#### 1. Introduction

### 1.1. Silicon in marine biogeochemical cycles

Silicic acid (Si(OH)<sub>4</sub>, or dissolved Si) is a bio-limiting nutrient in the ocean (Broecker and Peng, 1982; Dugdale et al., 1995). It is essential for the growth of a variety of marine organisms including diatoms, silico-flagellates, some Rhizaria (including radiolaria) and sponges. The oceanic silicon cycle has been comprehensively reviewed, most recently by Treguer and De La Rocha (2013). Global oceanic bSi production is estimated to be 240 ± 40 Tmol Si year<sup>-1</sup> and is mainly attributed to diatoms (Nelson et al., 1995). With a compositional Si: C molar ratio of 0.13 (Brzezinski, 1985), diatoms also contribute 30–40% of the primary production occurring in the surface ocean (DeMaster, 2003), closely intertwining the marine carbon and silicon cycles. A large fraction of the diatom frustles and other biogenic Si (bSi) dissolves in the upper water column. The rest is exported to the deep ocean as particles, with the majority of the bSi rain at 1 km reaching the ocean floor (Hammond et al., 2004). Much of the bSi rain to the seabed then remineralizes in

the upper sediments, transforming to silicic acid that diffuses back to the overlying water. It is eventually carried back to the euphotic zone and re-used for new diatom growth.

The diagenesis of bSi in the water column and seabed has been extensively studied (DeMaster, 2003), yet there is significant spatial variability and large uncertainties for flux estimations (Nelson et al., 1995; Treguer and De La Rocha, 2013). Although intense biogeochemical Si cycling has been recognized mainly at continental margins and the Southern Ocean, a compilation of sediment trap data at 2000 m depth has suggested high export fluxes of biogenic opal also occur within the North Pacific Subarctic Gyre (Honjo et al., 2008), which differs from other open ocean systems where the intensity of Si cycling is considerably lower (e.g. the North Atlantic). There are few measurements of benthic Si fluxes between 130°W and 180°E, 20°N and 55°N (Treguer and De La Rocha, 2013); we provide a latitudinal transect in this sector of the N. Pacific.

<sup>\*</sup> Corresponding author. Department of Earth Sciences, University of Southern California, 3651 Trousdale Pkwy Los Angeles, CA, 90089, USA. E-mail address: yihou@rice.edu (Y. Hou).

<sup>&</sup>lt;sup>1</sup> Present address: Department of Earth, Environmental and Planetary Sciences, Rice University, MS-126, 6100 Main Street, Houston, TX 77005, USA

# 1.2. North Pacific double silica maxima

The deep Northeast Pacific water column has two silica maxima. This unique feature was first described by Edmond et al. (1979), and it was hypothesized that the dissolution of opaline sediments alone could create the near-bottom increase, although no benthic flux estimates for the region were available at the time. Talley and Joyce (1992) published a more comprehensive set of water column data. They noted that an intermediate-depth silica maximum is present, characterized by a plume of high silicic acid concentration extending from the Cascadia Basin between 2 and 3 km in the North Pacific deep waters, while a bottom silica maximum exists only in a narrow meridional range (approximately between 140 and 160°W) in the subpolar region (Talley and Joyce, 1992). They proposed several possible causes for the water column structure, but the underlying dynamics that create the double silica maxima are not yet well understood. The flux required to sustain the North Pacific Intermediate Si anomaly has been estimated by Johnson et al. (2006), although its source has not been clearly determined. Further studies using coupled Ge/Si analysis ruled out the possibility that hydrothermal input introduced in Cascadia Basin is the source of the intermediate depth anomaly (Esther et al., 2010). Despite efforts to constrain the source of the intermediate silica maximum, there is little data focusing on the bottom maximum at high latitudes in the North Pacific.

Notably, the bottom maximum is found in a region that is roughly coincident with the eastern North Pacific subarctic gyre, where intense silica production and cycling are inferred to occur in the upper ocean (Gnanadesikan, 1999). However, no data is available on the gross bSi production in the subarctic gyre. A rough estimation of 10 Tmol Si/year (Treguer and De La Rocha, 2013) was made based on sediment trap measurements (Honjo et al., 2008) assuming the fraction remineralized in the upper ocean is similar to the Southern Ocean (Nelson et al.,

2002). Furthermore, there is little data available to illuminate how much of this production reaches the sea floor and is recycled, which would help better define the global biogeochemical cycling of Si. As one of the distinct features in the subarctic North Pacific, the bottom silicic acid maximum is worth further investigation.

In this study, water column, porewater and sediment samples were retrieved along a transect near 150°W from Hawaii to Alaska, in order to quantify the benthic Si fluxes and to investigate potential correlations between bSi production in surface water and the bottom Si maximum. Benthic diffusive silicic acid fluxes were estimated with both core incubations and porewater profile models. These fluxes were compared with the concentration gradients observed in the deep water column to examine whether benthic diffusive fluxes could be the primary source of the bottom silicic acid maximum. Sediment samples were analyzed for biogenic silica content; bSi burial fluxes were then estimated, which, jointly with benthic flux estimates, further constrain the Si budget of the North Pacific. The spatial correlation between the benthic Si rain to the seabed and the upper ocean production was also investigated for potential coupling between benthic remineralization and surface production.

# 2. Study area

Water and sediment samples were collected at five sites (Fig. 1) along a North Pacific transect near 150°W during Aug. 1–30, 2017 on the research cruise CDisK-IV aboard the R/V Kilo Moana. Stations 1–3 are in the North Pacific subtropical gyre where downwelling dominates. Stations 4–5 are in the subarctic gyre where upwelling brings cold, nutrient-rich deep water to the photic zone where nutrients can be used for phytoplankton growth. This continuous supply of nutrients by upwelling accounts for the significantly higher productivity in the subarctic gyre. The Transition Zone Chlorophyll Front (TZCF), a basin-scale

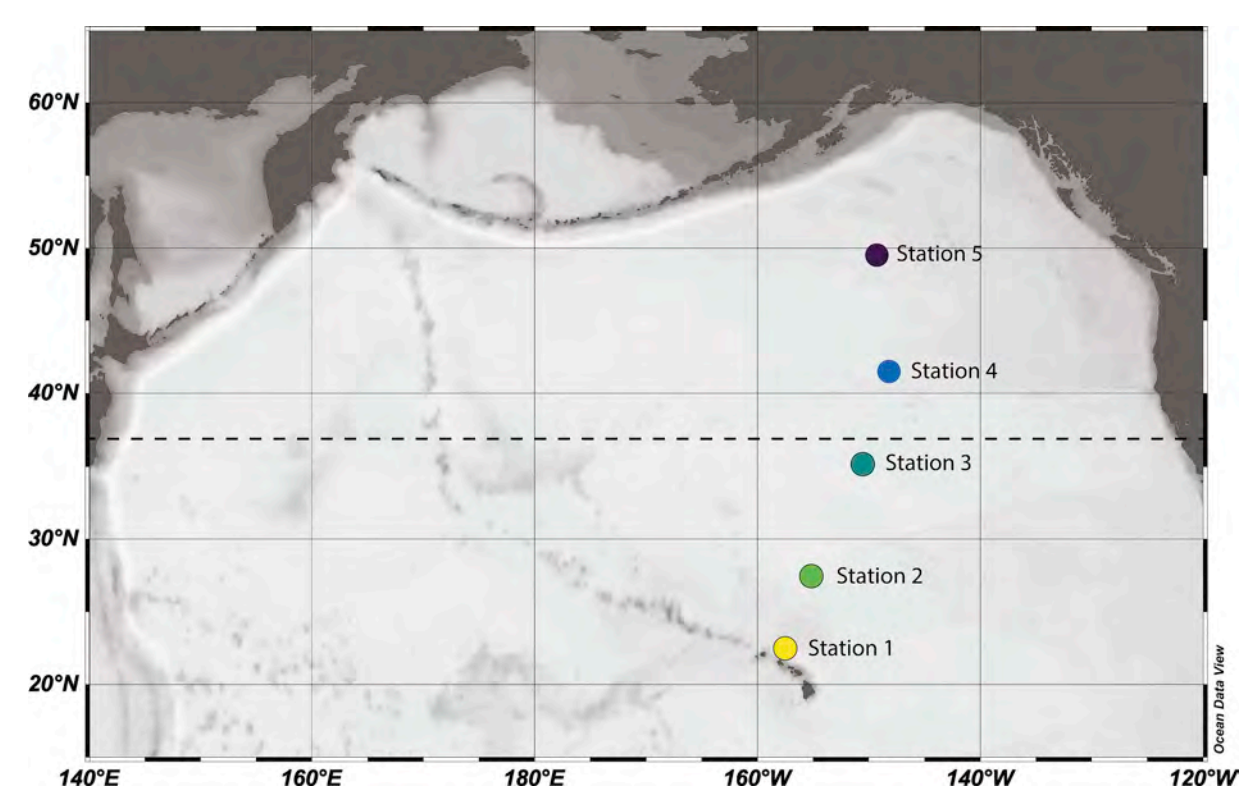


Fig. 1. Map of the study area. Dashed line marks the Transition Zone Chlorophyll Front (TZCF) at the time of the cruise (Dungenne, personal communication).

**Table 1**Station information, estimated Si fluxes, and porewater response time parameters (see section 5.1 for details).

Station	Lat (°N)	Long (°W)	Bottom	Porosity <sup>a</sup>	Si diffusive flux	(mmol m <sup>-2</sup> day	<sup>-1</sup> )	bSi burial flux -(µmol m <sup>-2</sup>	Burial Efficiency (%)	β (cm <sup>-1</sup> )		
			Depth (m)		Incubation			Porewater	day <sup>-1</sup> )	Efficiency (%)		Constant (day)
					Core A	Core B	Average					
1	22° 45.9′	157° 58.5′	4830	0.865	$-0.02 \pm 0.01$	$0.00 \pm 0.01$	$-0.01 \pm 0.01$	$0.04 \pm 0.01$	0.4	0.90	0.20	77.6
2	27° 45.8′	155° 15.3′	5741	0.823	$-0.03 \pm 0.01$	$0.00 \pm 0.01$	$-0.01 \pm 0.01$	$0.04 \pm 0.01$	0.3	0.71	0.35	30.2
3	35° 16.8′	150° 59.8′	5565	0.855	$-0.04 \pm 0.03$	$-0.02 \pm 0.03$	$-0.03 \pm 0.03$	$0.05 \pm 0.01$	0.4	0.79	0.39	21.7
4	41° 43.5′	148° 17.5′	4970	0.887	$0.80 \pm 0.02$	$0.74 \pm 0.01$	$0.77 \pm 0.02$	$0.56 \pm 0.14$	6.7	0.99	1.01	2.9
5	49° 50.4′	149° 37.7′	4783	0.784	$0.54 \pm 0.02$	$0.37 \pm 0.02$	$0.46 \pm 0.02$	$0.33~\pm~0.08$	21.3	5.12	0.75	7.7

<sup>&</sup>lt;sup>a</sup> Porosity is measured as the porosity of 0-1 cm sediments.

chlorophyll front that migrates seasonally between the subarctic-subtropical transition zone between 32°N (winter) and 42°N (summer), defines the dynamic boundary between low and high surface chlorophyll in the North Pacific (Polovina et al., 2001, 2017; Juranek et al., 2012) and tracks the seasonal movement of the physical boundary between the subarctic and subtropical gyres (Ayers and Lozier, 2010). The TZCF was located at 37°N on the CDisK-IV cruise, based on the fluorescence data and high-resolution particle size spectra collected with an Underwater Vision Profiler (UVP) (Dungenne, personal communication). Stations 3 and 4 straddle this transition zone, Station 3 primarily on the sub-tropical boundary and Station 4 within the sub-Arctic boundary.

Location and depth of the five stations are provided in Table 1. Sediment conditions differ slightly at each station. Sediments are very fine-grained clays at Station 1–4 and are grittier at Station 5. Worm tubes were visible at the sediment surface at Stations 1 and 5. Manganese nodules were abundant at Station 2, 3 and 5. A fluff layer above the water-sediment interface was observed at Station 4 (Supp. Fig. 1) and was considered to be recent biogenic debris that fell from the surface ocean, indicative of recent high surface production and rapid export to depth (Agusti et al., 2015).

# 3. Methods

# 3.1. Sample collection

At each station, sediment cores were retrieved using an Ocean Instruments 800 multi-corer with polycarbonate liners (i.d. = 9.6 cm), and cores were promptly placed in the cold van on board the R/V Kilo Moana. Two cores with undisturbed water-sediment interfaces were selected for core incubation. Incubations were done following the methodology of Hammond et al. (2004). Briefly, an incubation cap (Supp. Fig. 2a) was inserted into the core top, and the height of overlying water was adjusted to about 12 cm. The motor (30 rpm) was connected to a 12-V power source upon insertion of the incubation cap, to provide stirring. The configuration is shown in Supp. Fig. 2b. Cores were incubated at in situ temperature (~2°C) for 6-14 days, and 5-7 samples were taken periodically during the incubation. For each sampling, an aliquot of water (7 mL) was taken to flush the tubing and monitor the temperature, followed by collection of 40-45 mL that was filtered through a 0.45 µm PES syringe filter. Each sample draw lowered the core-top water height by about 0.6 cm.

A different sediment core with a pristine water-sediment interface was selected for porewater sampling. Rhizons (Rhizosphere Research Products) were inserted through pre-drilled apertures at  $\sim\!2\,\mathrm{cm}$  depth intervals and attached to evacuated syringes (Normject) to extract water. These samples were taken about 4–8 h after core retrieval, to let Si equilibrate between solid and dissolved phases at in situ temperature. About 10 mL pore water was collected with each rhizon, although the

volumes varied due to sediment heterogeneity.

Another sediment core was selected for sectioning. Sediments were sectioned at 1-2 cm intervals within 24-72 h of core retrieval. The sediment samples were later subsampled and analyzed for porosity (by water weight loss, assuming salinity of 34.7% and sediment density of  $2.5 \, \text{g/cm}^3$ ) and biogenic silica content (bSi) in the laboratory (see below).

Water column samples were collected with Niskin bottles on a CTD rosette at each station. A 50 mL aliquot of seawater was sampled from each Niskin bottle, immediately filtered and refrigerated for nutrient analysis.

# 3.2. Artifact and adjustments

Temperatures recorded throughout the incubations indicate a relatively constant cold room temperature of  $2.3\pm1.2\,^{\circ}\mathrm{C}$ , although the temperature of each individual core was dependent on its proximity to the compressor and the traffic in and out of the cold room. As a result, the average incubation temperature of each core was compared against the *in situ* temperature of bottom water to correct for a temperature effect when calculating the flux, making an adjustment of 6% per degree Celsius for silicic acid as recommended by Hammond et al. (2004). The total adjustment was never more than 10%.

Due to loosened tie-down lines, cores Sta. 1A, Sta. 1B and Sta. 2B were found to have fallen 2h after incubation started at Station 2 (four days after Sta. 1 incubation began). Upon discovery, the mounting rack was re-fastened and the cores re-secured vertically. Although no water loss was visible, minor leakage could have happened. The sediment-water interfaces must have been slightly disturbed, as slopes of 20–25° were observed. This disturbance was expected to accelerate the fluxes; the subsequent sampling was therefore delayed, letting sediments to resettle. However, the nutrient data for these cores showed no evidence of disturbance or increased flux.

# 3.3. Biogenic silica analysis

Biogenic silica contents in the sediments were determined with an alkaline leaching method modified from DeMaster (1981) and Mortlock and Froelich (1989). Briefly, 0.1–0.15 g dry, ground sediment samples were leached with 50 mL 5% Na<sub>2</sub>CO<sub>3</sub> solution at 80 °C in a water bath. Duplicate samples of leachate were taken at time zero (before samples were heated) as a blank, and after 3, 4, 5 h. The dissolved Si concentrations were analyzed and plotted against time. The amount of Si released from biogenic silica in the sediment was determined as the difference between y-axis intercept (time zero) of a linear regression to the 3-, 4-, and 5-h samples and the blank. This leaching procedure is not particularly effective for robust radiolarians (DeMaster, 1981), but microscopic analysis of the biogenic silica separated from sediments at Station 5 (not reported in this paper) suggests that the predominant bSi

is diatom. Results are reported as weight percent  $SiO_2$ , based on a molecular weight of  $60\,g/mole$ .

#### 3.4. Nutrient analysis

Silicic acid concentrations of water column, incubation and porewater samples were measured on board the R/V Kilo Moana, while leaches were analyzed in the laboratory, following procedures of Parsons et al. (1984), with a Hitachi U-1100 UV/Vis spectrophotometer. Measurements of duplicate samples indicate the precision for silicic acid was 1%.

#### 4. Results

#### 4.1. Core incubation

The calculations of benthic silicic acid fluxes were done as previously described in Hammond et al. (2004). The dissolved Si concentration change in the overlying water was plotted against the sum of elapsed time over water height (Fig. 2), where the slope equals the dissolved silica flux:

$$J = \frac{\Delta C \cdot V}{S \cdot \Delta t} = \frac{\Delta C}{\Sigma (\Delta t_i / h_i)} \tag{1}$$

where  $\Delta C$  is the change of dissolved Si concentration;  $\Delta t_i$  is the time elapsed for each interval; S is the surface area of the core; V is the volume of overlying water; and  $h_i$  is the overlying water height for each interval.

The relatively linear trends seen in the plots (Fig. 2) suggest that the Si fluxes were nearly constant throughout the incubation; therefore, linear regressions were used to determine the slopes (fluxes) and corresponding uncertainties.

Fluxes are reported as the average of two incubated cores (Table 1):  $0.01 \pm 0.01$ ,  $-0.01 \pm 0.01$ ,  $-0.03 \pm 0.03$ ,  $0.77 \pm 0.02$ , and  $0.46 \pm 0.02$  mmol Si m<sup>-2</sup> day<sup>-1</sup> through Station 1 to 5. The uncertainties are further discussed in section 5.1.

#### 4.2. Porewater analyses

The porewater silicic acid profiles (Fig. 3) show large gradients in the upper sediments and approach asymptotic values near depths of 10 cm. Compared with stations at lower latitudes, Stations 4 and 5 have higher silicic acid concentrations at the water-sediment interface and steeper, larger gradients. To calculate silicic acid fluxes from porewater data, each profile was first fitted with an exponential equation (McManus et al., 1995):

$$C = C_d - (C_d - C_0)\exp(-\beta z)$$
(2)

where C is the silicic acid concentration as a function of depth z (cm);  $C_0$ ,  $C_d$ , and  $\beta$  are fitting parameters:  $C_0$  is the dissolved Si concentration at the water-sediment interface and  $C_d$  is the dissolved Si concentration when z approaches infinity. The diffusive flux of silicic acid across the water sediment interface was then calculated using Fick's first law:

$$J = -\phi^3 D_0 \left(\frac{dC}{dz}\right)_0 \tag{3}$$

where  $\phi$  is the porosity of the sediments 0–1 cm below the water-sediment interface;  $D_0$  is the molecular diffusivity of silicic acid at *in situ* temperature of 1.6 °C (5.5×10<sup>-6</sup> cm<sup>-2</sup> s<sup>-1</sup>, Wollast and Garrels, 1971; McManus et al., 1995); and  $\left(\frac{dC}{dz}\right)_0$  is the concentration gradient at the water-sediment interface (z = 0). The tortuosity effect on diffusivity has been incorporated by the term  $\phi^3$  (Ullman and Aller, 1982).

Estimated fluxes are 0.04  $\pm$  0.01, 0.04  $\pm$  0.01, 0.05  $\pm$  0.01, 0.56  $\pm$  0.14, and 0.33  $\pm$  0.08 mmol Si m<sup>-2</sup> day<sup>-1</sup> from Station 1 to 5 (Table 1).

# 4.3. Burial of biogenic silica

Fig. 4 presents the profiles of biogenic silica contents as weight percent bSi (assuming it is stoichiometric  $SiO_2$  as noted in methods). At Stations 1–3, bSi contents are around 1% and show little variation with depth, while bSi is much higher at Stations 4 and 5 (3.0% and 7.7% at 0–1 cm sediment interval, respectively). Despite scatter and relatively

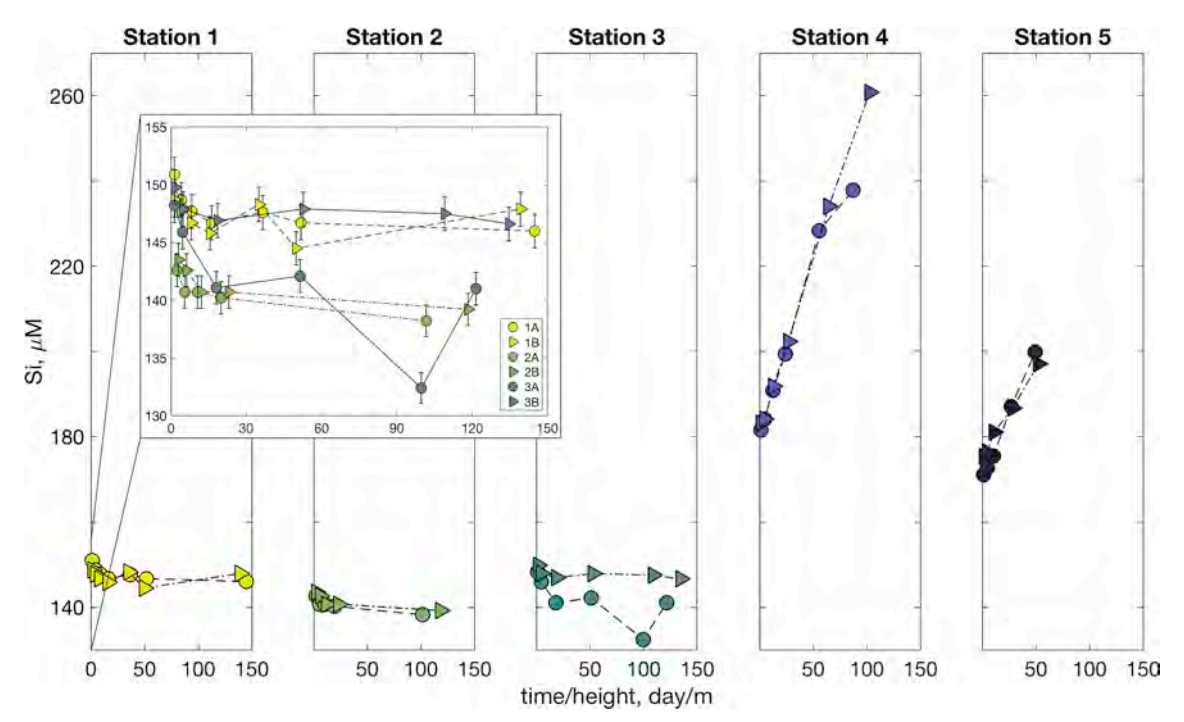


Fig. 2. Incubation results. Error bars are not shown when they are about the size of the data points.

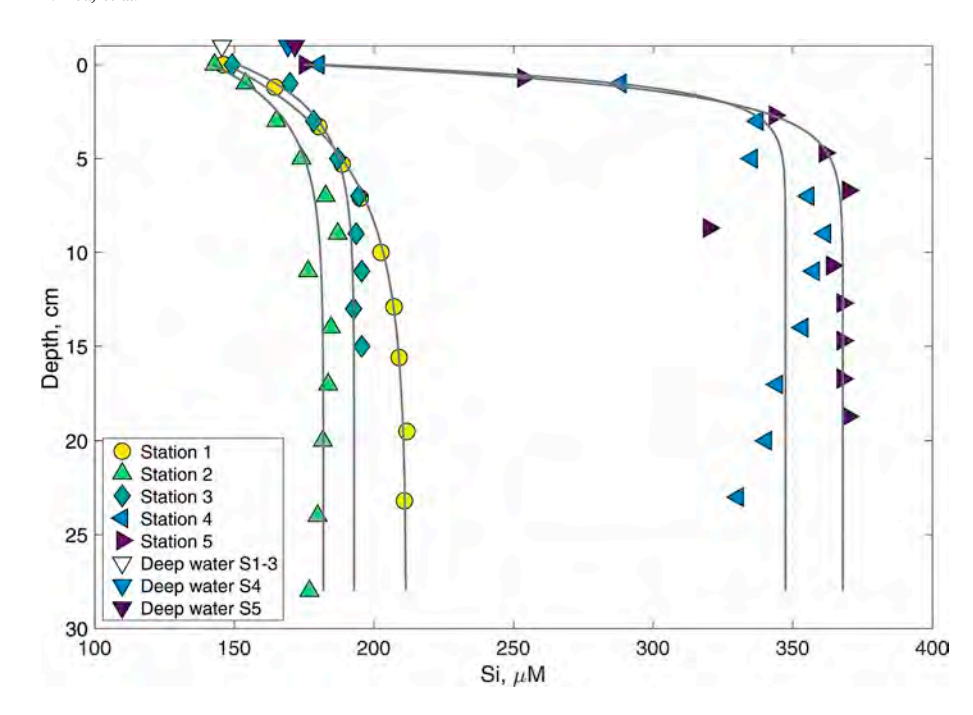


Fig. 3. Porewater profiles of silicic acid concentration, exponential fits shown in grey lines. Data points plotted at depth zero are core-top water Si concentrations. Bottom water (from CTD casts) Si concentrations are plotted for reference (depth not to scale); Si concentrations at Station 1–3 are indistinguishable in the figure therefore plotted as one data point.

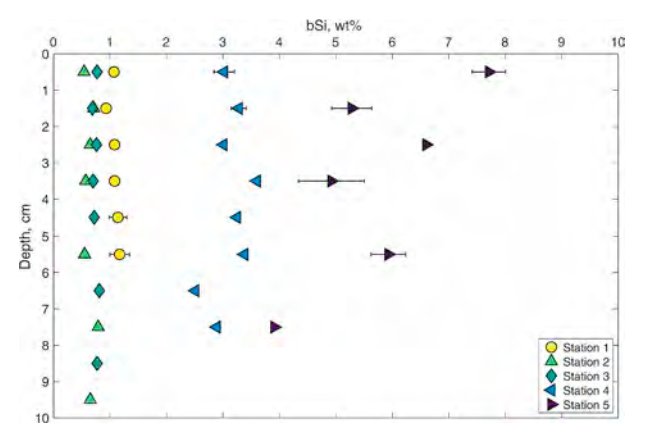


Fig. 4. Profiles of biogenic silica content in sediments in wt% SiO<sub>2</sub>.

large uncertainties, bSi content generally decreases with depth at Station 5, perhaps due to stronger bioturbation relative to dissolution, compared to Station 1–4 where no bSi gradient was observed. Because both porewater profiles and solid phase bSi indicate most dissolution occurs in the upper 1 cm, the average bSi content below 1 cm at each station was used to calculate the burial flux:

$$J_{burial} = \frac{\rho(1-\phi)}{m_{bSi}} \cdot f \cdot LSR \tag{4}$$

where  $\rho$  and  $\phi$  are the density and porosity of the sediments, respectively; LSR is the linear sedimentation rate;  $m_{bSi}$  is the molecular weight of bSi; and f is the average weight fraction of bSi below 1 cm in the sediments. For this calculation, we used linear sedimentation rates estimated from paleomagnetic data found in Opdyke (1970) as long-term regional averages for the past 700kyr. However, due to the limited spatial resolution of their data (and perhaps temporal variation in accumulation rates), the rate at each station could have an uncertainty of x2. Based on interpolation between their data points for proximal stations, rates of 0.2, 0.2, 0.3, 1.5, 1.5 cm/kyr were chosen for Station 1 to 5, respectively. Preliminary estimates based on excess  $^{230}$ Th profiles in the upper 5 cm of stations 2 and 3 (Kemnitz, unpublished) are

comparable to these estimates. Estimated bSi burial fluxes are shown in Table 1.

The burial efficiency of bSi can be calculated, assuming all biogenic silica that reaches the seafloor as particle rain would either dissolve or be preserved:

$$burial\ efficiency(\%) = 100 \times \frac{bSi\ burial\ flux}{bSi\ burial\ flux + DSi\ diffusive\ flux} \tag{5}$$

The burial efficiencies are around 1% for Station 1 to 4, while 5% of biogenic silica is preserved in the sediments at Station 5 (Table 1).

#### 5. Discussion

#### 5.1. Constraining the benthic Si fluxes

Negative fluxes with 100% uncertainties were calculated in the incubation cores at Stations 1, 2, and 3, although it is evident from the porewater profiles that a diffusive flux into the sediments is very unlikely. The unrealistic incubation results probably reflect the limitation of the technique for detecting extremely low fluxes. Based on fluxes calculated from porewater profiles at the subtropical stations, the change in silicic acid concentration in the core-top water would be as low as  $2\,\mu\text{M}$  for a 10-day incubation period, which is almost indistinguishable from the analytical uncertainty of  $1.5\,\mu\text{M}$  (1% of the starting core-top water concentration of  $\sim 150\,\mu\text{M}$ ).

While the uncertainties of incubation estimates can be taken as the uncertainties of the linear regressions, the uncertainties involved in porewater flux estimations are more difficult to quantify. The largest uncertainties are associated with the positions of rhizons relative to the sediment-water interface. As shown in Fig. 3, the calculated concentration gradient is rather sensitive to the depths and concentrations of porewater samples above 2 cm. Therefore, it is important to insert the rhizons horizontally, which they were. Each rhizon may draw porewater from a depth range (Seeberg-Elverfeldt et al., 2005), limiting sample resolution. However, uncertainties in the exponential fits of porewater profiles are relatively small, despite these uncertainties; porewater profiles were fitted well with Equation (2) (Fig. 3) with the exception of deeper intervals at Station 4. With porosities of about 0.9 and porosity uncertainties of less than 3%, less than 10% uncertainties

in flux calculations are expected (Eq. (3), note the cubic relationship between flux and porosity). Considering these factors, an overall 25% uncertainty was assigned to the porewater flux estimations.

The benthic Si fluxes estimated by core incubation and porewater profiles agree within  $\pm 2\sigma$  of their uncertainties. Fluxes estimated with incubation are systematically higher at Station 4 and 5 than those estimated with porewater profiles. This might be a result of some bioirrigation at these sites: benthic organisms might mix the overlying water with porewater by burrowing, enhancing the vertical transport of silicic acid above diffusive fluxes. It is more likely that a non-steady state situation might also cause some discrepancy between porewater and incubation estimates. As mentioned earlier, the recent biogenic debris (fluff laver) observed at the core top at Station 4 possibly reflected a recent bloom in the surface ocean. While the incubation experiment would respond rather quickly to dissolution of fresh biogenic debris, it should take a longer time for the porewater profile to respond to a recent input of reactive bSi. An estimate of pore water response times can be made by considering the parameter  $\beta$  from fits with Eq. (2). McManus et al. (1995) have shown that one interpretation of this parameter leads to a rate constant for pore water equilibration k, based on previously defined parameters:

$$k = \phi^3 D_0 \beta^2 \tag{6}$$

Time constants (as 1/k) for Stations 1 to 5 indicate decreasing response time with higher latitude, which range from less than a week to 2 months (Table 1), possibly leading to some mismatch between fluxes determined from incubations and pore waters. Seasonality in the intensity of upper ocean Si cycling has been observed in the subarctic Pacific (Takahashi et al., 2000) and at Station ALOHA (our Station 1; Karl et al., 2012), with the highest export likely in spring and early summer. At a settling speed of  $\sim 100 \, \text{m/day}$  (Smetacek, 1985), particle fluxes to the seabed should have a built-in phase lag of 1–2 months following upper ocean changes. Due to the low sensitivity of the incubation technique, fluxes based on porewater profiles are adopted as the best estimate for Stations 1–3, while an average of the two techniques is adopted for Stations 4 and 5.

# 5.2. Deep water circulation and the double silicic acid maxima

Double silica maxima were observed at Stations 4 and 5 (Fig. 5); prominent maxima were near  $\sim\!2000$  m and more subtle maxima in the deepest bottom water,  $\sim\!5000\,\text{m}.$  Assuming one-dimensional diffusive transport, silicic acid fluxes in the lower water column can be calculated as:

$$J_{water\ column} = -\frac{dC}{dz}K_Z \tag{7}$$

where  $\frac{dC}{dz}$  is the concentration gradient in the lower water column and  $K_z$  is the eddy diffusivity. In the bottom 500 m, the concentration gralinear dients were estimated with regressions  $6.6{\times}10^{-3} \pm 5.0{\times}10^{-3}\,\mu\text{M/m}$  and  $8.4{\times}10^{-3}\,\mu\text{M/m}$  (uncertainty unavailable due to low data resolution) for Station 4 and Station 5. To match the previously estimated benthic fluxes, apparent eddy diffusivities required by Eq. (7) would be 11.7 cm<sup>2</sup>/s and 5.5 cm<sup>2</sup>/s (uncertainties of a factor of two). Analyses of <sup>227</sup>Actinium in the lower 500 m of the water column were also made on this cruise and used to independently estimate K<sub>z</sub> (Kemnitz, 2018). The <sup>227</sup>Ac profiles indicate very high K<sub>z</sub> in the lower 500 m, approaching 20 cm<sup>2</sup>/s, and similar to those calculated from the silicic acid budgets. However, above the lower 500 m, where density gradients become larger, <sup>227</sup>Ac profiles

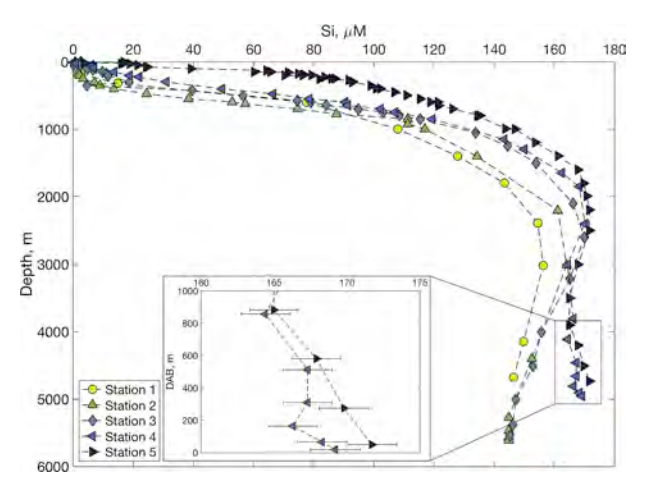


**Fig. 5.** Water column silicic acid profiles. Note that silicic acid concentrations are plotted against depth above bottom (DAB) in the inset. Uncertainties in the inset are  $\pm 1\sigma$ .

indicate  $K_z$  appears to be  $< 1\,\mathrm{cm}^2/\mathrm{s}$ . If solute transport is primarily vertical, the lower eddy diffusivity should lead to a corresponding increase in the concentration gradient of silicic acid above 500 m, a change that is clearly absent in the water column profiles. The low silicic acid gradients more than 500 m above the bottom require that horizontal transport in the water column must remove both Si and Ac from these waters, preventing silicic acid from diffusing further upward.

Weak diapycnal mixing in this region was also reported by Hautala (2018), where inverse modeling was used to resolve abyssal overturning circulation in the North Pacific. These observations emphasize the critical role of horizontal transport in regulating distributions of solutes released by sedimentary remineralization in this region of the North Pacific, and its role in controlling the double maxima in silicic acid water column profiles.

#### 5.3. Burial efficiency for bSi and bSi rain rates

Burial fluxes and bSi dissolution rates (diffusive + burial fluxes) at each station define the rain of bSi to the seafloor and were used to find burial efficiency (Eq. (5)). The efficiency at Station 5 ( $\sim$ 5%) is higher than Stations 1–4 ( $\sim$ 1%), although the uncertainties associated with sedimentation rate estimates introduce uncertainties of at least a factor of two in the estimates for these stations. Despite the uncertainties, the burial efficiencies are very low, since almost all bSi rain is remineralized, so the uncertainty in accumulation rate has little effect on bSi rain estimates at our study sites.

All available benthic Si flux estimates from the N. Pacific are compiled in Table 2. Burial fractions (Eq. (5)) were calculated where sufficient data is available and then plotted against bSi rain rates (Fig. 6). Results indicate the burial fraction is relatively constant for the region and shows no consistent trend with bSi rain rate, despite the factor of 10 range in the latter. A North Pacific basin-scale average burial efficiency of 2.8% was obtained from this data assemblage, in close agreement with previously estimated global average of 3% (Nelson et al., 1995).

**Table 2**Compilation of North Pacific benthic Si fluxes (in mmol m<sup>-2</sup> year<sup>-1</sup>).

Reference	Location <sup>a</sup>	Lat	Long	Date	Method <sup>¶</sup>	Bottom Depth	Diffusive Flux	Burial Flux	bSi Rain (2000m)	bSi Rain (seafloor) <sup>c</sup>	Burial Efficiency
		(°N)	(°E)			(m)	_				(%)
Esther et al. (2010)	Cacadia Basin	40.5	-126.0	2006 Aug	CI, SL	3113	307	14.6		321	4.5
		42.0	-125.2	2006 Aug	CI, SL	3090	358	14.6		372	3.9
		42.6	-125.3	2006 Aug	CI, SL	3063	365			<u>376</u>	
		43.6	-127.3	2006 Aug	CI, SL	2922	241	7.3		248	2.9
		45.1	-125.6	2006 Aug	CI, SL	2923	274	14.6		288	5.1
		45.1	-126.2	2006 Aug	CI, SL	2738	223			229	
		45.1	-126.5	2006 Aug	CI, SL	2838	245			<u>252</u>	
		45.1	-127.5	2006 Aug	CI, SL	2842	303	14.6		318	4.6
		45.1	-129.1	2006 Aug	CI, SL	2798	376	14.6		391	3.7
		46.4	-128.0	2006 Aug	CI, SL	2750	234	10.95		245	4.5
		47.5	-127.2	2006 Aug	CI, SL	2622	343			<u>353</u>	
Shibamoto and Harada,	Northwest	50.0	165.0	1999 May	PWC, SL	5510	241	3		244	1.2
2010	Pacific	44.0	155.1	1998-2000	PWC, SL	5333	305	8.9		314	2.8
		36.0	146.6	1998 Aug	PWC, SL	5679	389	1		390	0.3
		30.2	135.0	2003 May	PWC, SL	4427	77	3		80	3.4
This study	Northeast	22.5	-157.6	2017 Aug	PWR, CI, SL	4830	15	0.1		15	0.9
•	Pacific	27.5	-155.2	2017 Aug	PWR, CI, SL	5741	15	0.1		15	0.7
		35.2	-150.6	2017 Aug	PWR, CI, SL	5565	18	0.1		18	0.8
		41.4	-148.2	2017 Aug	PWR, CI, SL	4970	243	2		245	1.0
		49.5	-149.4	2017 Aug	PWR, CI, SL		144	8		152	5.1
Honjo et al. (2008) and	PSAG-W	51.5	-145.0	1991	Trap				1229	1168	
references therein	PSAG-W		165.0	1997	Trap				343	326	
	PSAG-W		175.3	1993	Trap				779	740	
	PSAG-W		165.1	1991	Trap				619	588	
	PSAG-W		155.0	1989	Trap				511	485	
	PSAG-W		155.0	1997	Trap				568	540	
	NPST-E		175.0	1993	Trap				95	90	
	NPST-E		177.7	1993	Trap				34	<u>32</u>	
	NPST-E		175.0	1993	Trap				23	22	
	PSAG-E	50.0		1983	Trap				253	240	
	PSAG-E	49.0	-174.0	1995	Trap				294	279	
	NPPF	45.1	-176.9		Trap				161	153	
	NPTG	31.7	-124.6		Trap				18	17	
	NPTG	15.4	-151.5	1978	Trap				10	10	
Suess et al. (1998)	Aleutian	57.3	-148.0		PWU	4744	255 <sup>b</sup>			263	

Method abbreviations: CI: core incubation; SL: sediment leaching; PWC: porewater extracted by centrifuge; PWR: porewater extracted by rhizons; Trap: sediment trap: PWU: porewater (unspecified extraction method).

<sup>&</sup>lt;sup>c</sup> Bolded and underlined numbers are calculated assuming 95% of bSi that reaches 2 km would reach seafloor, 2.8% of which would get buried. For details see section 5.3.

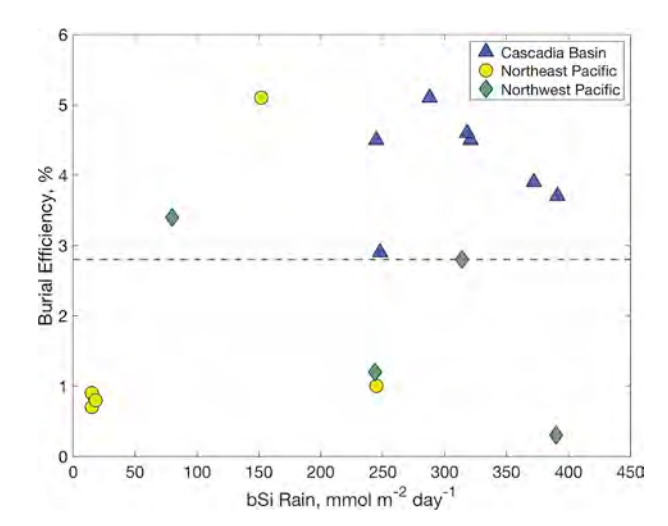


**Fig. 6.** Burial efficiency vs. bSi rain rates. Data from Cascadia Basin (Esther et al., 2011), Northwest Pacific (Shibamoto and Harada, 2010) and Northeast Pacific (this study). Dashed line indicates a North Pacific basin-scale average burial efficiency of 2.8% (global average: 3%).

# 5.4. Coupling of benthic remineralization with surface production

Net Community Production (NCP) of oxygen within the surface mixed layer (usually 10–15 m) along the same transect has been previously measured (Juranek et al., 2012) and is compared with the rain rates of bSi to the seabed (Fig. 7). The positions of the Transition Zone Chlorophyll Front (TZCF) when the two sets of data were collected were approximately the same. Benthic Si fluxes show good correlation with NCP of oxygen: both oxygen production and benthic fluxes are small in the subtropical gyre and increase significantly near the TZCF.

On a basin scale, the rain of bSi to the sea floor can be compared to surface production. The estimate of 3% burial efficiency was used to calculate the benthic rain of bSi where only pore water estimates of remineralization were available. If only sediment trap rain of bSi at 2 km was available, rain to the sea floor was estimated using the assumption that 95% of the biogenic silica that reaches 2 km would reach the seafloor (Hammond et al., 2004). The estimated bSi rain rates were then compared with annual average sea surface chlorophyll data (Fig. 8). Although the data resolution of bSi rain rates is low, the overall distribution of high production regions is successfully reproduced in the contour map, where high rain rates of biogenic silica rain correspond to

<sup>&</sup>lt;sup>a</sup> Location abbreviations (adopted from Honjo et al., 2008): NPPF (North Pacific Polar Front), NPST-E (North Pacific Subtropical Gyre-East), PSAG-W (Pacific Subarctic Gyre-West), NPTG (North Pacific Tropical Gyre).

<sup>&</sup>lt;sup>b</sup> Calculated based on porewater profile (Suess et al., 1998) with an assigned bottom water silicic acid concentration of 170??M (typical for the region); porewater data above 6 cm were used to estimate the concentration gradient.

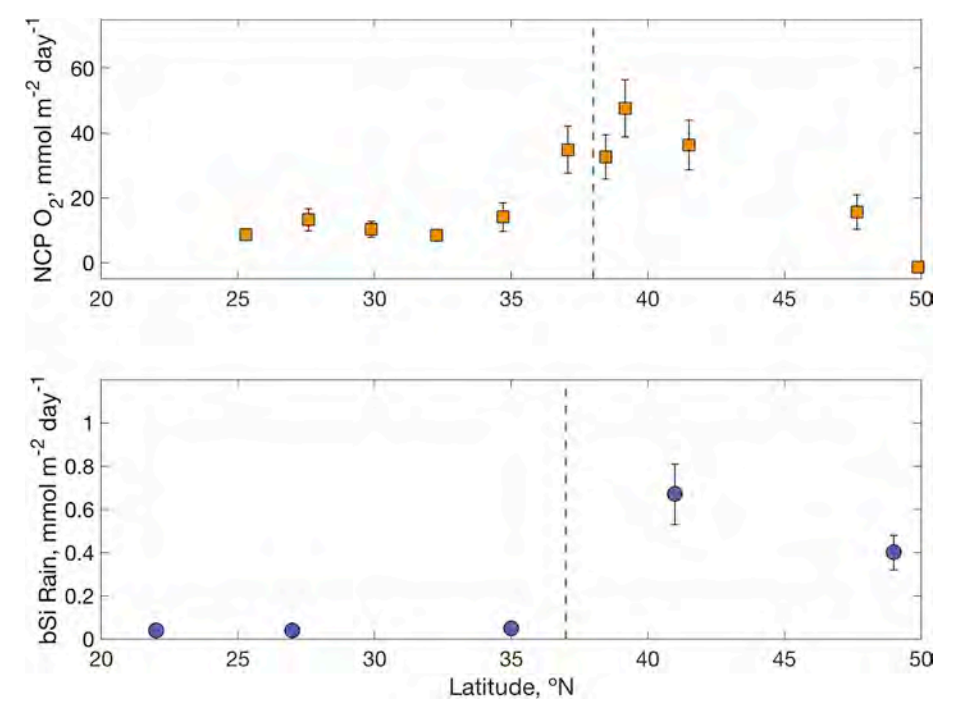
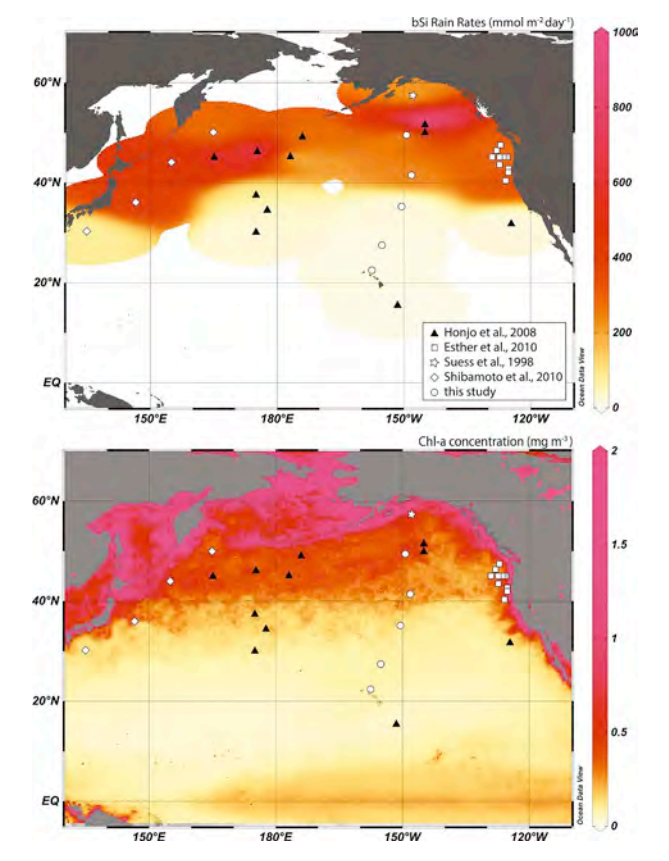


Fig. 7. Comparison between Net Community Production (NCP) from surface mixed layer oxygen supersaturation, measured during a cruise in Oct. 2003 along a transect near  $155^{\circ}W$  (Juranek et al., 2012), and biogenic Si rain to the seabed. Dashed lines mark the position of Transition Zone Chlorophyll Front (TZCF) as shown by Juranek et al. (upper panel) and on this cruise in 2017 (lower panel); the TZCF may migrate seasonally by about  $\pm$  4° from these positions.



**Fig. 8.** Upper panel shows the contour map made from bSi rain rate compilation (Table 2). Lower panel shows annual average sea surface chlorophyll concentration for 2017 (NASA MODIS, 2018). Symbols indicate locations of bSi rain estimations. Open symbols indicate bSi rain rates estimated from benthic fluxes; filled symbols are estimates from sediment trap data (for details see section 5.3).

high surface chlorophyll concentrations.

At Station ALOHA (Sta. 1), the benthic remineralization of Si represents about 20% of the Si export flux from the surface ocean

 $(0.18 \pm 0.11 \,\mathrm{mmol}\,\mathrm{m}^{-2}\,\mathrm{day}^{-1};\,\mathrm{Brzezinski}\,\mathrm{et}\,\mathrm{al.},\,2011).\,\mathrm{This}\,\mathrm{fraction}$ is comparable to, but lower than the average export efficiency (33%) for the Pacific sector of the Southern Ocean (Nelson et al., 2002). It seems a bit surprising that these settings with rather different upper ocean temperature characteristics have similar export efficiencies. This might reflect a modest contribution of deeper dwelling Rhizaria to the vertical flux, but may simply reflect the ability of a similar fraction of rapidly sinking particles to rain into cooler, deep waters in both environments. If the silicon cycle at the North Pacific subarctic gyre operates at efficiencies similar to the Antarctic and ALOHA, an annual bSi production of the subarctic gyre could be estimated. Extrapolating the average benthic bSi rain rates north of 40°N presented in Table 2 (365 mmol m<sup>-2</sup> day<sup>-1</sup>) to a region of 6.1 million km<sup>2</sup> (Longhurst et al., 1995) with a range of export efficiencies calculated (0.22-0.33), indicates 6.75-10.12 Tmol Si year<sup>-1</sup>. This value is consistent with previous estimates for this region of 10 Tmol Si year<sup>-1</sup> (Treguer and De La Rocha, 2013), using a somewhat smaller database.

# 6. Conclusion

Along a North Pacific transect near 150°W from 22°N to 50°N, the benthic silica fluxes estimated with two independent approaches, core incubation and porewater profile modeling, agree within uncertainties. Observed burial efficiencies of biogenic silica are comparable with previous estimates in other parts of the North Pacific. These average about 3%, indicating remineralization of the bSi rain is practically complete, with little variance across the region despite high uncertainties introduced by poorly constrained sedimentation rates.

In the North Pacific subarctic gyre (Stations 4 and 5), the ratio of silicic acid benthic fluxes to silicic acid concentration gradients observed through the bottom 500 m of the water was used to estimate apparent eddy diffusivities through this depth range. Results are consistent with apparent eddy diffusivities estimated from  $^{227}\mathrm{Ac}$  profiles through this depth range, suggesting benthic remineralization is likely the primary source of the near-bottom silicic acid increase in the subarctic North Pacific. However, in water above  $\sim\!500\,\mathrm{m}$  from the bottom, apparent eddy diffusivity is much lower, but silicic acid concentration gradients are too small to match the benthic input, indicating significant loss of silicic acid and other solutes remineralized in the

seabed, due to horizontal transport.

Biogenic silica rain rates to the sea floor show a spatial pattern that is very similar to that of sea surface chlorophyll concentration. The rain exhibits a spatial pattern that reflects upper ocean production, where high rain rates below the subarctic gyre correspond with high diatom production in the surface water.

# Acknowledgment

Financial support was provided by NSF Grants OCE1436958 and OCE1260692 to D.E. Hammond, OCE1220302 to W.M. Berelson, and a USC Provost's Undergraduate Research Fellowship to Y. Hou. The assistance of the Captain, crew and science team of R/V Kilo Moana (KM 1712) in field work is greatly appreciated. We thank two anonymous reviewers for insightful comments that have helped to improve the manuscript, and Susanne Neuer is thanked for editorial handling.

# Appendix A. Supplementary data

Supplementary data to this article can be found online at https://doi.org/10.1016/j.dsr.2019.04.013.

#### References

- Agusti, S., González-Gordillo, J.I., Vaqué, D., Estrada, M., Cerezo, M.I., Salazar, G., Gasol, J.M., Duarte, C.M., 2015. Ubiquitous healthy diatoms in the deep sea confirm deep carbon injection by the biological pump. Nat. Commun. 6 (1), 7608. https://doi.org/10.1038/ncomms8608.
- Ayers, J., Lozier, M., 2010. Physical controls on the seasonal migration of the North Pacific transition zone chlorophyll front. J. Geophys. Res.: Oceans 115 (C5). https://doi.org/10.1029/2009JC005596.
- Broecker, W.S., Peng, T.H., Lamont-Doherty Geological Observatory, 1982. Tracers in the Sea. Palisades, N.Y.
- Brzezinski, M.A., 1985. The Si: C: N ratio of marine diatoms: interspecific variability and the effect of some environmental variables. J. Phycol. 21 (3), 347–357. https://doi.org/10.1111/j.0022-3646.1985.00347.x.
- Brzeziński, M.A., Krause, J.W., Church, M.J., Karl, D.M., Li, B., Jones, J.L., Updyke, B., B, 2011. The annual silica cycle of the North Pacific subtropical gyre. Deep-Sea Res. Part I 58 (10), 988–1001. https://doi.org/10.1016/j.dsr.2011.08.001.
- DeMaster, D.J., 1981. The supply and accumulation of silica in the marine environment. Geochem. Cosmochim. Acta 45 (10), 1715–1732. https://doi.org/10.1016/0016-7037(81)90006-5.
- DeMaster, D.J., 2003. The diagenesis of biogenic silica: chemical transformations occurring in the water column, seabed, and crust. In: In: MacKenzie, F.T. (Ed.), Treatise on Geochemistry, vol. 7. pp. 87–98. https://doi.org/10.1016/B0-08-043751-6/07095-X.
- Dugdale, R.C., Wilkerson, F.P., Minas, H.J., 1995. The role of a silicate pump in driving new production. Deep Sea Res., Part I 42, 697–719. https://doi.org/10.1016/0967-0637(95)00015-X.
- Edmond, J.M., Jacobs, S.S., Gordon, A.L., Mantyla, A.W., Weiss, R.F., 1979. Water column anomalies in dissolved silica over opaline pelagic sediments and the origin of the deep silica maximum. J. Geophys. Res.: Oceans 84 (C12), 7809–7826. https://doi. org/10.1029/JC084iC12p07809.
- Esther, T.A., Hammond, D.E., Hautala, S.L., Johnson, H.P., Schwartz, R.J., Paukert, A.N., 2010. Evaluation of the budget for silicic acid in Cascadia Basin deep water. Deep-Sea Res. I 57, 677–686. https://doi.org/10.1016/j.dsr.2010.02.002.
- Gnanadesikan, A., 1999. A global model of silicon cycling: sensitivity to eddy parameterization and dissolution. Glob. Biogeochem. Cycles 13 (1), 199–220. https://doi.org/10.1029/1998GB900013.
- Hammond, D.E., Cummins, K.M., McManus, J., Berelson, W.M., Smith, G., Spagnoli, F., 2004. Methods for measuring benthic nutrient flux on the California margin: comparing shipboard core incubations to in situ lander results: shipboard versus in situ benthic fluxes. Limnol Oceanogr. Methods 2 (6), 146–159. https://doi.org/10.4319/ lom.2004.2.146.
- Hautala, S.L., 2018. The abyssal and deep circulation of the Northeast Pacific basin. Prog. Oceanogr. 160, 68–82. https://doi.org/10.1016/j.pocean.2017.11.011.
- Honjo, S., Manganini, S.J., Krishfield, R.A., Francois, R., 2008. Particulate organic carbon fluxes to the ocean interior and factors controlling the biological pump: a synthesis of

- global sediment trap programs since 1983. Prog. Oceanogr. 76 (3), 217–285. https://doi.org/10.1016/j.pocean.2007.11.003.
- Johnson, H.P., Hautala, S.L., Bjorklund, T.A., Zarnetske, M.R., 2006. Quantifying the North pacific silica plume. Geochem. Geophys. Geosyst. 7 (5) N/a.. https://doi.org/ 10.1029/2005GC001065.
- Juranek, L.W., Quay, P.D., Feely, R.A., Lockwood, D., Karl, D.M., Church, M.J., 2012. Biological production in the NE Pacific and its influence on air-sea CO<sub>2</sub> flux: evidence from dissolved oxygen isotopes and O<sub>2</sub>/Ar. J. Geophys. Res. 117, C05022. https:// doi.org/10.1029/2011JC007450.
- Karl, D.M., Church, M.J., Dore, J.E., Letelier, R.M., Mahaffey, C., 2012. Predictable and efficient carbon sequestration in the North Pacific Ocean supported by symbiotic nitrogen fixation. Proc. Natl. Acad. Sci. U. S. A 109 (6), 1842–1849. https://doi.org/ 10.1073/pnas.1120312109.
- Kemnitz, N.J., 2018. Actinium-227 as a Tracer for Mixing in the Deep Northeast Pacific. M.S. Thesis. University of Southern California, pp. 110pp.
- Longhurst, A., Sathyendranath, S., Platt, T., Caverhill, C., 1995. An estimate of global primary production in the ocean from satellite radiometer data. J. Plankton Res. 17 (6), 1245–1271. https://doi.org/10.1093/plankt/17.6.1245.
- McManus, J., Hammond, D.E., Berelson, W.M., Kilgore, T.E., Demaster, D.J., Ragueneau, O.G., Collier, R.W., 1995. Early diagenesis of biogenic opal: dissolution rates, kinetics, and paleoceanographic implications. Deep Sea Res. II: Topical Studies in Oceanography 42 (2), 871–903. https://doi.org/10.1016/0967-0645(95)00035-O.
- Mortlock, R.A., Froelich, P.N., 1989. A simple method for the rapid determination of biogenic opal in pelagic marine sediments. Deep Sea Res. Part A, Oceanographic Research Papers 36 (9), 1415–1426. https://doi.org/10.1016/0198-0149(89) 90092-7
- NASA Goddard Space Flight Center, Ocean Ecology Laboratory, Ocean Biology Processing Group Moderate-resolution Imaging Spectroradiometer (MODIS) Aqua Chlorophyll Data, 2018. Reprocessing. NASA OB. DAAC, Greenbelt, MD, USA. https://doi.org/10.5067/AQUA/MODIS/L3M/CHL/2018, Accessed date: 5 September 2018.
- Nelson, D.M., Treguer, P., Brzezinski, M.A., Leynaert, A., Queguiner, B., 1995. Production and dissolution of biogenic silica in the ocean: revised global estimates, comparison with regional data and relationship with biogenic sedimentation. Glob. Biogeochem. Cycles 9, 359–372. https://doi.org/10.1029/95GB01070.
- Nelson, D.M., Anderson, R.F., Barber, R.T., Brzezinski, M.A., Buesseler, K.O., 2002. Vertical budgets for organic carbon and biogenic silica in the Pacific sector of the Southern Ocean, 1996–1998. Deep-Sea Res.II 49, 1645–1674. https://doi.org/10. 1016/S0967-0645(02)00005-X.
- Opdyke, N.D., Foster, J.H., 1970. In: Hays, J.D. (Ed.), Paleomagnetism of Cores from the North Pacific, in Geological Investigations of the North Pacific. Geological Society of America, Boulder, Colo, pp. 83–119.
- America, Boulder, Colo, pp. 83–119.

  Parsons, T.R., Maita, Y., Lalli, C.M., 1984. A Manual of Chemical and Biological Methods for Seawater Analysis. Pergamon Press, pp. 25–28.
- Polovina, J.J., Howell, E.A., Kobayashi, D.R., Seki, M.P., 2001. The transition zone chlorophyll front, a dynamic global feature defining migration and forage habitat for ma- rine resources. Prog. Oceanogr. 49 (1), 469–483. https://doi.org/10.1016/ S0079-6611(01)00036-2.
- Polovina, J.J., Howell, E.A., Kobayashi, D.R., Seki, M.P., 2017. The transition zone chlorophyll front updated: advances from a decade of research. Prog. Oceanogr. 150, 79–85. https://doi.org/10.1016/j.pocean.2015.01.006.
- Seeberg-Elverfeldt, J., Schluter, M., Feseker, T., Kolling, M., 2005. Rhizon sampling of pore waters near the sediment-water interface of aquatic systems. Limnol Oceanogr. Methods 3, 361–371. https://doi.org/10.4319/lom.2005.3.361.
- Shibamoto, Y., Harada, K., 2010. Silicon flux and distribution of biogenic silica in deep-sea sediments in the western North Pacific ocean. Deep-Sea Res. I 57 (2), 163–174. https://doi.org/10.1016/j.dsr.2009.10.009.
- Smetacek, V., 1985. Role of sinking in diatom life-history cycles: ecological, evolutionary and geological significance. Mar. Biol. 84, 239–251. https://doi.org/10.1007/ BF00392493.
- Suess, E., Bohrmann, G., Huene, R.V., Linke, P., Wallmann, K., Lammers, S., Sahling, H., Winckler, G., Lutz, R.A., Orange, D., 1998. Fluid venting in the eastern aleutian subduction zone. J. Geophys. Res. 103 (B2), 2597–2614. https://doi.org/10.1029/ 97JB02131.
- Takahashi, K., Fujitani, N., Yanada, M., Maita, Y., 2000. Long-term biogenic particle fluxes in the Bering Sea and the central subarctic Pacific Ocean, 1990–1995. Deep-Sea Res. I 47 (9), 1723–1759. https://doi.org/10.1016/S0967-0637(00)00002-9.
- Talley, L.D., Joyce, T.M., 1992. The double silica maximum in the North Pacific. J. Geophys. Res. 97 (C4), 5465–5480. https://doi.org/10.1029/92JC00037.
- Treguer, P., De La Rocha, C.L., 2013. The world ocean silica cycle. Ann. Rev. Marine Science 5, 477–501. https://doi.org/10.1146/annurev-marine-121211-172346.
- Ullman, W., Aller, R., 1982. Diffusion coefficients in nearshore marine sediments. Limnol. Oceanogr. 27 (3), 552–556. https://doi.org/10.4319/lo.1982.27.3.0552.
- Wollast, R., Garrels, R.M., 1971. Diffusion coefficient of silica in seawater. Nat. Phys. Sci. (Lond.) 229, 94. https://doi.org/10.1038/physci229094a0.